

Article

Research on Casing Deformation Prevention Technology of a Deep Shale Gas Well Based on Cementing Slurry System Optimization

Jing Cao , Shangyu Yang *, Lihong Han *, Jianjun Wang, Yisheng Mou and Caihong Lu

State Key Laboratory for Performance and Structure Safety of Petroleum Tubular Goods and Equipment Materials, CNPC Tubular Goods Research Institute, Xi'an 710077, China

* Correspondence: yangshangyu@cnpc.com.cn (S.Y.); hanlihong@cnpc.com.cn (L.H.); Tel.: +86-29-81887661 (S.Y.); Fax: +86-29-88223416 (S.Y.)

Abstract: In the complex fracturing process of shale gas wells, casing is subjected to serious deformation, which can easily lead to the failure of wellbore integrity and the reduction of well construction productivity. It is particularly important to clarify the casing deformation mechanism and carry out effective control. Based on the logging data of casing deformation from well and full-scale indoor tests, the casing deformation mechanism is mainly considered to be shear and non-uniform extrusion deformation caused by formation slip and displacement control, i.e., the ultimate working conditions. The slip displacement boundary (<40 mm) under complex fracturing conditions is quantified to provide the design and optimization basis. Then, the influence laws of steel grade and wall thickness on the shear and non-uniform extrusion bearing characteristics are studied, using unconventional oil and gas well casing simulation test systems for 110 ksi ($\phi 139.7 \times 10.54$ mm) and 125 ksi ($\phi 139.7 \times 12.7$ mm) casings. Furthermore, combined with the full-scale simulation tests and finite-element simulation, the effects of elastic and modified cement slurry with hollow glass beads on casing deformation are compared and studied. The results show that the deformation capacity mitigation of casing is limited by reducing the cement elastic modulus and increasing the elastic cement thickness. By reasonably adding hollow glass beads of modified cement slurry, the maximum geological movement absorption of cement slurry is up to 27 mm. This new method can obviously decrease casing deformation and have an excellent control effect. Combined with the cementing technology of Luzhou blocks, the formula of modified cement slurry is optimized, and the optimization window of the casing deformation control process is formed, which can ensure the smooth progress of engineering fracturing.

Keywords: shale gas; casing deformation; cement slurry; shearing; external extrusion

Citation: Cao, J.; Yang, S.; Han, L.; Wang, J.; Mou, Y.; Lu, C. Research on Casing Deformation Prevention Technology of a Deep Shale Gas Well Based on Cementing Slurry System Optimization. *Processes* **2022**, *10*, 1678. <https://doi.org/10.3390/pr10091678>

Academic Editors: Sheng Yang, Jinze Xu, Desheng Zhou, Xing Hao and Zhangxing John Chen

Received: 9 June 2022

Accepted: 23 July 2022

Published: 24 August 2022

Publisher's Note: MDPI stays neutral with regard to jurisdictional claims in published maps and institutional affiliations.



Copyright: © 2022 by the authors. Licensee MDPI, Basel, Switzerland. This article is an open access article distributed under the terms and conditions of the Creative Commons Attribution (CC BY) license (<https://creativecommons.org/licenses/by/4.0/>).

1. Introduction

Significant shale gas reserves exist in China, and exploration and development has officially become the main growth point of the oil industry. However, in the complex fracturing process of shale gas wells, the casing is subjected to complex stress states and serious deformation, which affects the drilling cycle, increases well construction cost and reduces well construction productivity. Compared to North America, shale gas in southwest China generally has characteristics of deep burial, significant mountain structure and strong non-uniformity of in situ stress, so the service environment of the casing is very harsh. According to statistics, especially for horizontal wells, the casing deformation rate is up to 30% in the Sichuan Basin of China. Therefore, casing deformation has become a major bottleneck in China's shale gas development, and effective control methods are urgently needed.

According to the special geological characteristics and operating conditions of the southwest shale gas block, it is particularly important to study the deformation mechanism

and prevention measures for shale gas well casing. Experts and scholars have done a lot of research on the causes and mechanisms of casing deformation. In view of the casing deformation during and after the fracturing of a shale gas well, Daneshy [1] proposed that asymmetric fracturing is the main controlling factor of casing deformation, and the resulting differential compaction of reservoir produced shear stress, tensile stress and compressive stress along the interface, contributing to casing damage at the weakest interface.

Deenadayalu and Suarez-Rivera [2], Landry et al. [3], and Blake et al. [4] considered the integrity of the wellbore system, studied the variation law of wellbore circumferential stress during wellbore hydraulic fracture propagation in the fracturing process of a shale gas well, and proposed that the creep characteristics of a reservoir would lead to casing deformation. Wang et al. [5] determined that local buckling, connection failure and shear deformation are the main failure modes of casing. Through numerical simulation and logging information analysis, Hu et al. [6] believed that the deformation of segmented fracturing casing in a shale gas horizontal well was caused by formation shear slip, and the weak plane shear loss was mainly affected by elongation. They put forward a new cementing method and casing material, which could effectively alleviate the casing damage caused by formation slip. Carsero and Rylance [7] systematically analyzed casing deformation in a global shale gas development and believed that layer interface slippage and natural fault re-activation were the main causes of casing deformation.

Chinese researchers have also conducted a lot of research on shale gas casing deformation in southwest China. Based on the casing-cement sheath-stratum system in the hydraulic fracturing process of a shale gas well, Gao and Liu [8] discussed the influence law of the changes to the physical/mechanical parameters of casing and cement sheaths on the stress behavior of the system, and proposed that the deformation mechanism of casing was shear deformation, and that casing deformation was caused by the joint action of many factors such as fault or fracture sliding, temperature and pressure. By means of theoretical analysis, numerical simulation and field test, Yin et al. [9] revealed that the failure mechanism of casing in southwest shale gas wells was shear deformation caused by shear fracture sliding. Yan et al. [10] believed that formation sliding could not explain the casing deformation of a shale gas reservoir, and the uneven external stress of the casing after the decrease of cement pore pressure might be the main reason for the casing deformation. Liu et al. [11] thought that shale sliding, cement failure and micro-annuli caused by hydraulic fracturing of a shale gas well might generate local load, which would have a great impact on the stress state and anti-collapse strength of casing.

Although the problem of casing deformation and failure in shale gas wells has been observed in the past few years, and many researchers have tried to solve it, since there are so many factors attributed to this phenomenon, it is still a great challenge in the shale gas development process.

In terms of casing deformation prevention, Hu et al. [6] suggested using casing with a lower grade and smaller thickness on a weak surface to effectively reduce or delay casing damage. When the casing elongation increased by 60%, the critical failure slip displacement of casing could be increased by 21.40%. Liu et al. [11] used numerical simulation, Nesrter's method and field data analysis to show that local load and casing size have an important impact on casing failure. When φ is 90° , the local load area had the greatest influence on the collapse strength of casing. Increasing casing thickness and reducing casing outer diameter were beneficial to reducing casing damage in shale gas wells.

Lian et al. [12] thought that the prevention of casing deformation could not only be done by improving the steel grade and wall thickness of casing. The fracturing process was optimized by means of numerical analysis, and the view of reducing deformation by adjusting the parameters such as staged fracturing spacing was put forward. Yan et al. [10] believed that rotating the casing string during cementing to avoid the formation of cement pores, or using warm fracturing fluid to minimize the pressure drop in the pores, was a possible innovative strategy to solve these problems. Yin et al. [13] introduced casing curvature to evaluate the mobility and integrity of casing, reducing the crossing angle,

using cement with low Young's modulus, or even not cementing, which were effective measures to prevent casing damage. The cement sheath with low elastic modulus was used 2.0 m above and below the fault or natural fracture zone, and rubber and other particles were mixed to reduce the elastic modulus of the cement sheath to 1.0 GPa, which could effectively prevent the deformation of shale gas well casing. However, the problem of shale gas wellbore integrity still exists, and there are great differences in different blocks. There is a lack of reasonable and effective control methodology; therefore, it is necessary to carry out further research.

2. Casing Deformation Mechanisms of Complex Fracturing in Shale Gas Wells

Through multi-arm diameter detection of many shale gas casing deformation wells, the morphological characteristics of casing deformation can be obtained, which provides a research basis for preventing deformation. Figure 1 is a typical logging profile of casing deformation, which shows the extrusion deformation at multiple segments, while the transition zone between deformation and non-deformation or extrusion deformation shows shear morphology. This is mainly because in deep wells or wells with complex conditions, such as plastic creep formation of salt rock, cement string slots, casing eccentricity, irregular boreholes and too large dog legs will cause the casing string to suffer non-uniform external extrusion pressure, as described by Bai et al. [14] and Li et al. [15].

In the multi-stage fracturing process, due to the flow of fracturing fluid, it is easy to cause fault activation and local formation slip (Figure 1d), making the casing bear huge shear load and shear deformation, as described by Xu et al. [16]. Through the comparison between logging profile and indoor full-scale simulation experiment results, as shown in Figure 1b–e, the mechanisms of casing shear and extrusion deformation are determined, and the appearance of casing transformation has been verified.

Because the size of the shear area and extrusion area in the logging morphology is basically consistent with the corresponding size of the laboratory tests, and combined with the analysis of the formation cement sheath casing stress graph (Figure 1f), it is concluded that the casing deformation in the long horizontal section is mainly due to the shear and non-uniform extrusion deformation caused by the formation slip and displacement control, rather than the stress control.

Under actual underground working conditions, the service environment of the casing is harsh, and the stress states are complex. It is difficult to replicate limited experimental conditions as working conditions. Therefore, this paper mainly focuses on the main factors causing casing deformation, namely formation slip and displacement control, i.e., the ultimate working conditions, and studies the maximum diameter of casing under this ultimate working conditions. Furthermore, if the casing change prevention and control requirements in the ultimate working conditions are met, they are also met under other working conditions.

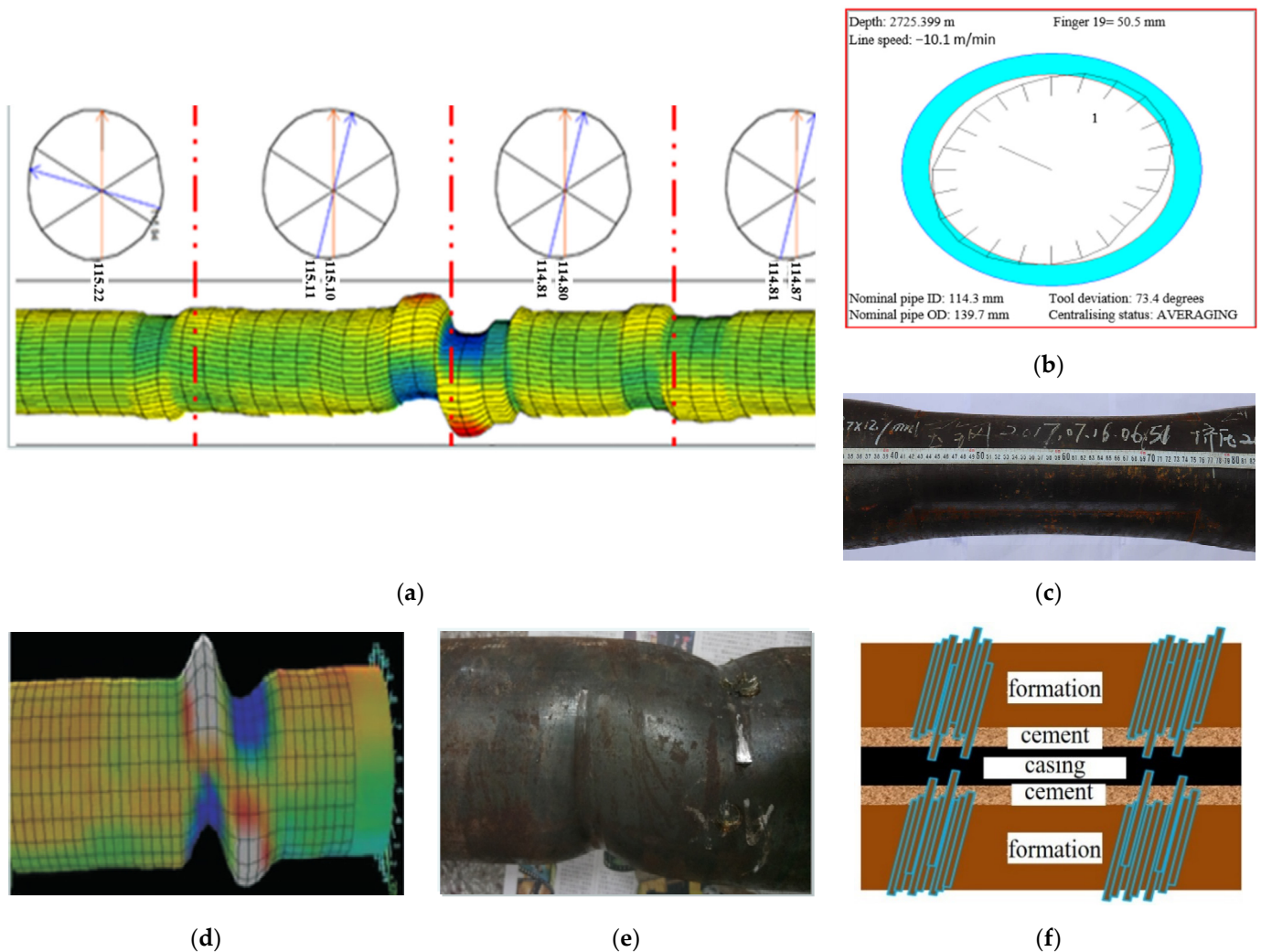


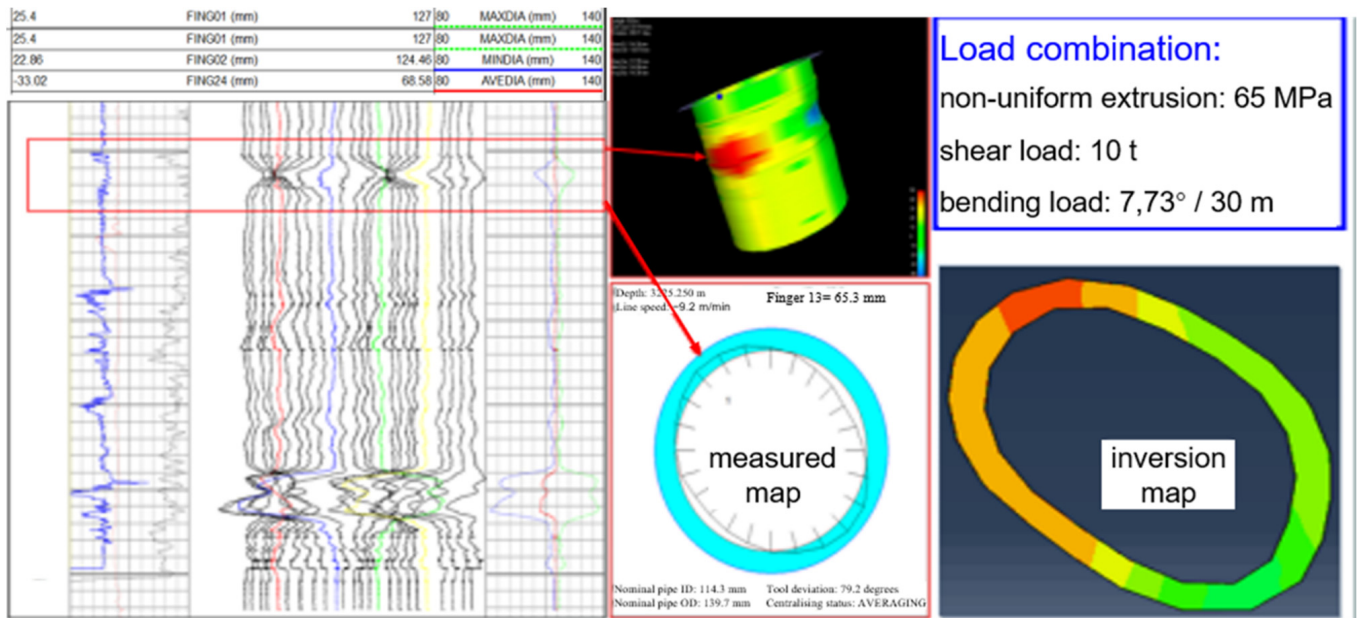
Figure 1. Typical deformation morphology of casing in a shale gas horizontal well: (a) logging morphology of a casing change well; (b) typical extrusion morphology; (c) extrusion test; (d) typical shear morphology; (e) shear test; (f) formation slip.

3. Determination of Casing Service Boundary Conditions in a Complex Fracturing Process

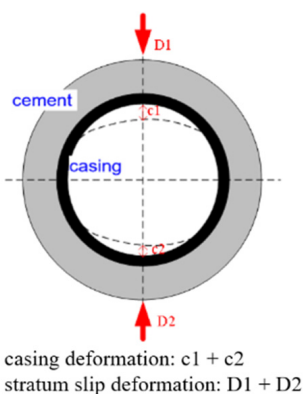
For casing deformation wells of shale gas, starting from logging data, with the help of numerical simulation and indoor simulation test verification, the radial casing variation inversion method can be established to obtain the statistical distribution law of casing variables. The size of reservoir casing in a typical casing change well is $\varnothing 139.7 \times 12.7$ mm, the steel grade is 125 ksi, and the logging curve of casing deformation section is shown in Figure 2a. It can be seen that the maximum deformation of inner diameter is 15 mm, and the corresponding deformation degree is 13.12%.

By establishing the finite-element model for simulation inversion, it is obtained that the corresponding formation slip is 20 mm, as shown in Figure 2b. The “unconventional oil and gas well casing string simulation test system” is used for the non-uniform external extrusion test of a full-size casing-cement sheath. When the extrusion displacement is 20 mm, the maximum deformation of inner diameter is 15.2 mm, as shown in Figure 2c. The reliability of the finite-element model in this paper is verified by the test. Using the same method, the corresponding formation slip of each set of deformation wells can be determined. Here, the elastic modulus of 125 ksi casing is 210 GPa, Poisson’s ratio is 0.3, yield strength is 957 MPa, and tensile strength is 1034 MPa. The water and lime ratio of conventional elastic cement

slurry is 0.5. After mixing and solidification, the elastic modulus is 9 GPa and Poisson's ratio is 0.25. When the cement is solidified for 7 days, the compressive strength is 19 MPa, and with the increase of time, the compressive strength increases.



(a)



(b)



(c)

Figure 2. Deformation well data analysis: (a) logging curve and simulation inversion; (b) casing deformation and formation slip; (c) test verification.

According to the logging results of multi-wall wells in the Luzhou block, Sichuan, there are 32 deformation points, of which 78% are less than 30 mm and 22% are greater than 30 mm. Therefore, the set variables are concentrated within 30 mm. Using the numerical simulation and laboratory simulation test, the corresponding formation displacement is determined to be 40 mm, which is the boundary condition of wellbore design determined in this paper.

4. Non-Uniform Bearing Characteristics Study of Shale Gas Well Casing

The bearing characteristics of 110 ksi and 125 ksi casings commonly used in shale gas wells under non-uniform extrusion load and shear load conditions are studied to provide test data support for the complex fracturing of shale gas wells in southwest oil and gas fields.

4.1. Bearing Characteristics of Pure Casing under Shear Load Conditions

Casings of 110 ksi ($\phi 139.7 \times 10.54$ mm) and 125 ksi ($\phi 139.7 \times 12.7$ mm) are selected for shear tests. Two sections of 400 mm-long 110 ksi casing numbered #1 and #2 and one section of 400 mm-long 125 ksi casing are intercepted, and the “unconventional oil and gas well casing string simulation test system” is used for shear test, as shown in Figure 3a. Here, the influence of the pipe ends and the influence zone at the shear deformation need to be considered. Through the comparison of the shear deformation of 800 mm- and 400 mm-long casings (Figure 3b), it is found that the outer diameter of the two casings after deformation is the same, so the shear force influence area is almost the same. From an economic point of view, 400 mm-long casing is selected. The number of tests in each group with the same parameters is three to ensure the repeatability of the tests.

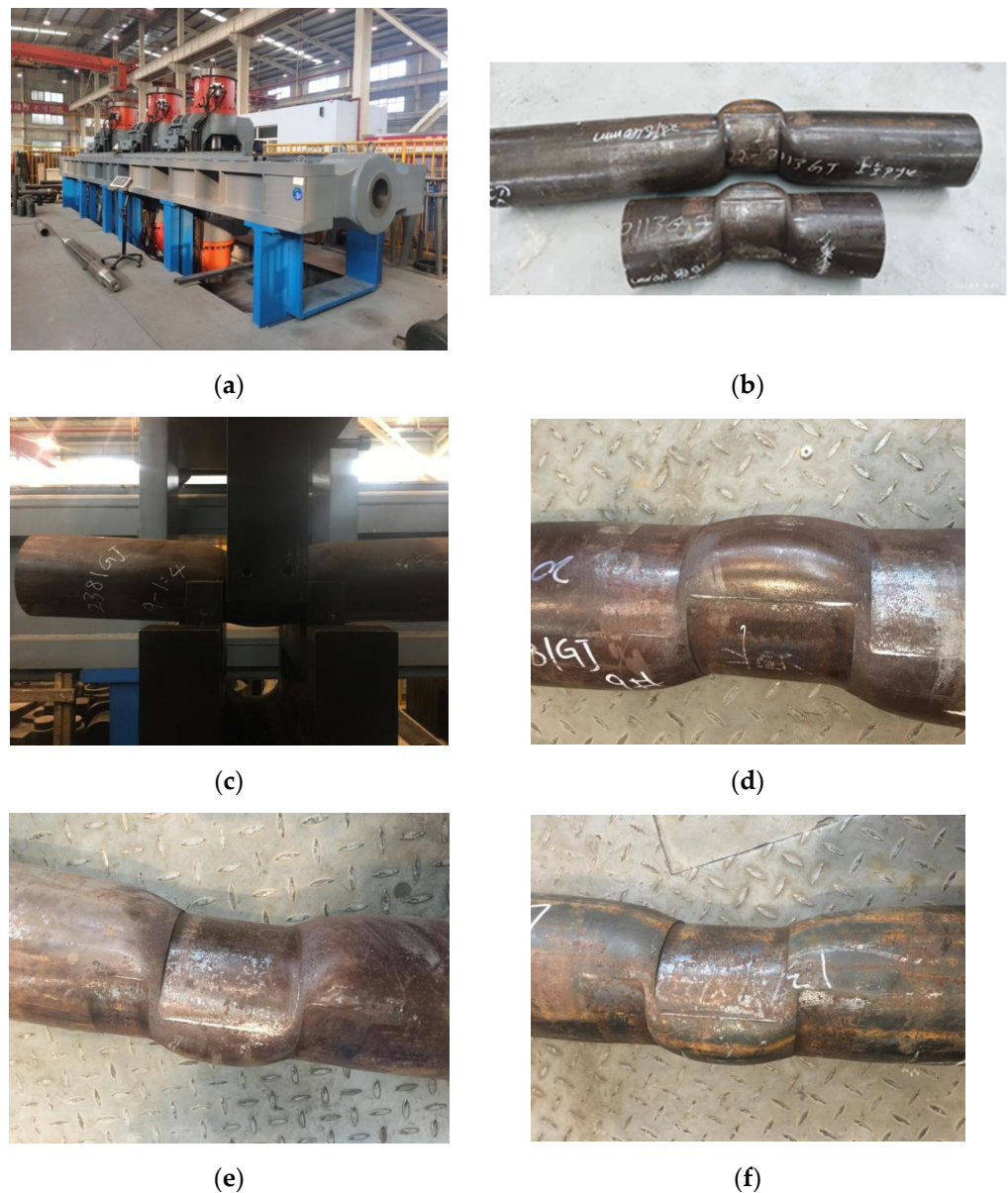


Figure 3. Morphology of casing after shear tests: (a) test device; (b) topography contrast; (c) shear test process; (d) #1 casing appearance after shear test; (e) #2 casing appearance after shear test; (f) 125 ksi casing appearance after shear test.

An ultrasonic thickness gauge is used to measure the wall thickness of four points evenly distributed in the ring of the cross-section, and the diameter in the pressure direction

and vertical direction at one half position of the pipe body is measured using vernier calipers. During the test, shearing is 15 mm and the shear load is recorded. The morphology of the casing is shown in Figure 3c–f, and the relationship between shear load and shear displacement is shown in Figure 4.

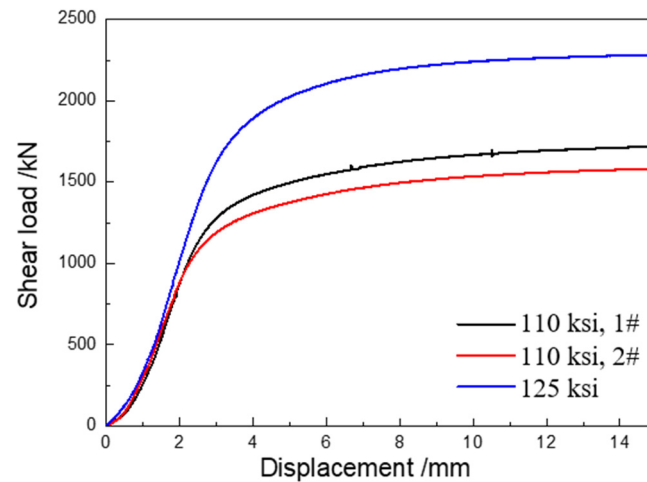


Figure 4. Curve of casing shear load and displacement.

From the above test results, it can be seen that the morphology of casing changes under shear force before and after shear test. The shear load increases with the increase of shear displacement. When the counter-shear is 15 mm, the shear load of 110 ksi casing is 1600 KN and that of 125 ksi casing is 2280 KN.

Based on ABAQUS 6.11 software, sourced from CNPC Tubular Goods Research Institute, Xi'an, China, 125 ksi ($\phi 139.7 \times 12.7$ mm) casing shear deformation is conducted by finite-element simulation. We take the well axis as the center, and take the 1200 mm-long casing structure as the calculation model. Due to the symmetry of the model, we take one half of the whole model as the calculation model in this paper. As shown in Figure 5, the outer diameter of the casing is 139.7 mm, and the wall thickness is 12.7 mm. The two ends of the casing and cement sheath are fully restrained, and the side is symmetrically restrained. The friction coefficient between the casing and cement is 0.2, and hexahedral grids are used. The Von Mises yielding criterion and isotropic hardening law are adopted.

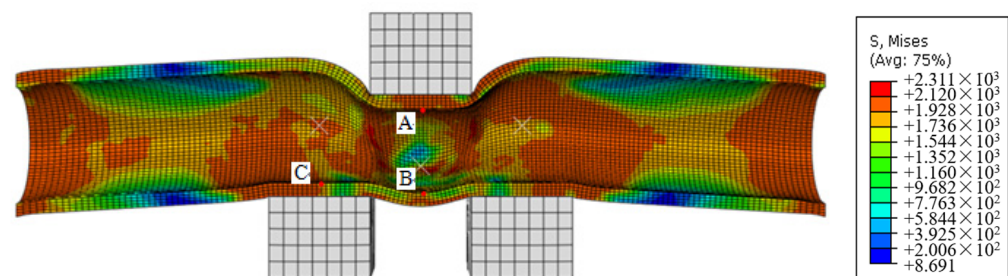


Figure 5. Cloud diagram of equivalent stress distribution after casing shearing: A is the uppermost end of the upper shear fixture; B is the lowest end; C is the uppermost end of the lower shear fixture.

The equivalent stress distribution of the pipe body after shearing for 20 mm is shown in Figure 5. Under non-uniform load, the equivalent stress distribution of the casing tends to be concentrated, and the maximum equivalent stress appears on the inner wall of the casing. Here, the minimum drift diameter is calculated, i.e., the distance AB from the uppermost end of the upper shear fixture to the lowest end, minus the transverse distance BC from the lowest end of the upper shear fixture to the uppermost end of the lower shear fixture. The minimum path is 80.51 mm and the deformation is 33.79 mm.

4.2. Bearing Characteristics of Cement Sheath-Casing under Shear Load Condition

Andrade and Sangesland [17] pointed out that a cement sheath has a direct impact on the stress load of casing. We select 110 ksi ($\phi 139.7 \times 10.54$) and 125 ksi ($\phi 139.7 \times 12.7$) casings to conduct cement sheath shear tests. Three sections of 400 mm-long 110 ksi casing numbered #1, #2, and #3 and one section of 400 mm-long 125 ksi casing are sheared for 15 mm and then the appearance and shear loads of the tested casing are analyzed.

The minimum outer diameter and outer diameter deformation value of the pipe body before and after the tests are shown in Figure 6. The finite-element numerical simulation data are shown in Figure 7. Both ends of the casing and cement are fixed, and the friction coefficient between casing and cement is 0.2. Compared with the shear of the pipe body, the equivalent stress after adding a cement sheath is significantly reduced, and the minimum drift diameter calculated by the same method is 82.08 mm. Compared with the shear minimum drift diameter of the pure pipe body of 80.51 mm, the drift diameter is increased by 1.57 mm, and the deformation of the minimum drift diameter is reduced by 1.95%.

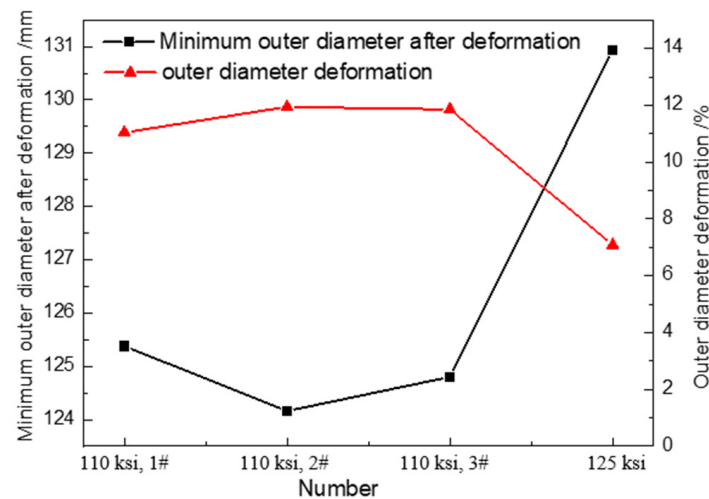


Figure 6. The minimum outer diameter and deformation of cement-sheath casing after shearing.

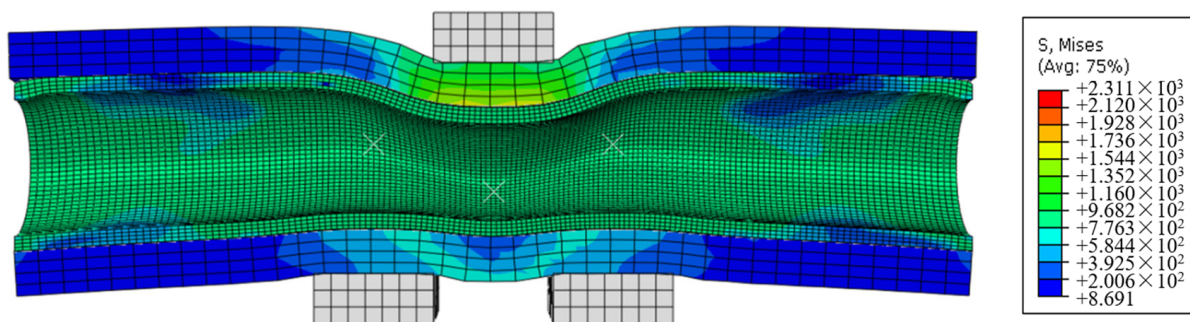


Figure 7. Equivalent stress distribution cloud of cement-sheath casing after shearing.

According to the analysis of test results, the outer diameter of 110 ksi ($\phi 139.7 \times 10.54$) and 125 ksi ($\phi 139.7 \times 12.7$) casings become smaller due to the shear force. Through measurement, it is found that the minimum outer diameter of the 110 ksi casing after shearing is 124.16 mm, the deformation value is 16.83 mm, and the maximum deformation is 11.94%; the minimum outer diameter of 125 ksi casing after shearing is 130.94 mm, the deformation value is 9.97 mm, and the deformation is 7.08%. Under the 30 mm shear displacement condition, the deformation of 110 ksi casing is 4.86% larger than that of 125 ksi casing. The morphology of casing after shear test is shown in Figure 8, and the relationship between shear load and shear displacement is shown in Figure 9.

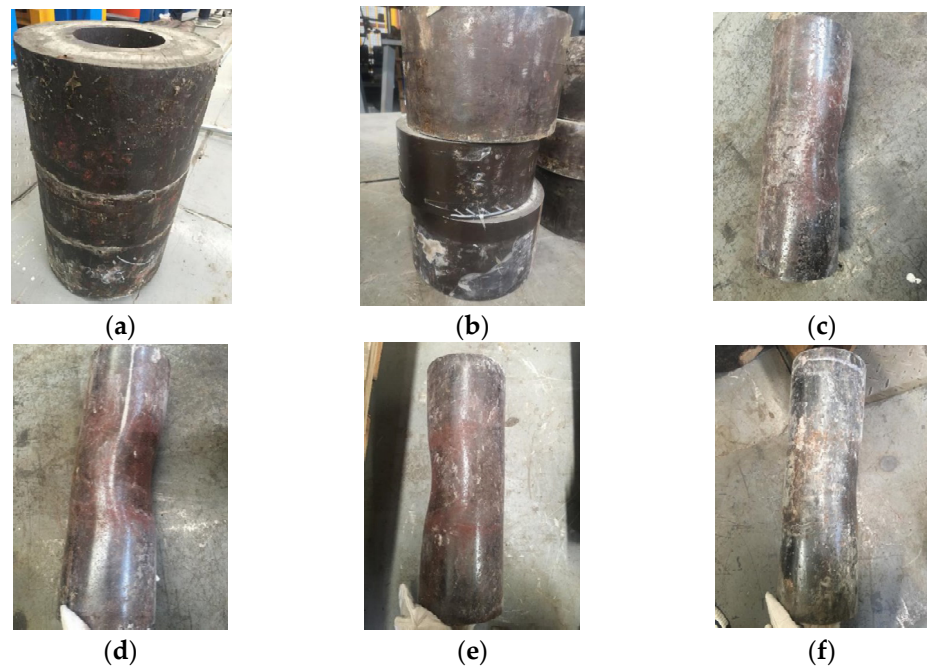


Figure 8. Appearance of cement sheath casing after shear test: (a) before cement sheath shear test; (b) After cement sheath shear test; (c) #1 cement-sheath casing after shearing; (d) #2 cement-sheath casing after shearing; (e) #3 cement-sheath casing after shearing; (f) 125 ksi cement sheath casing after shearing.

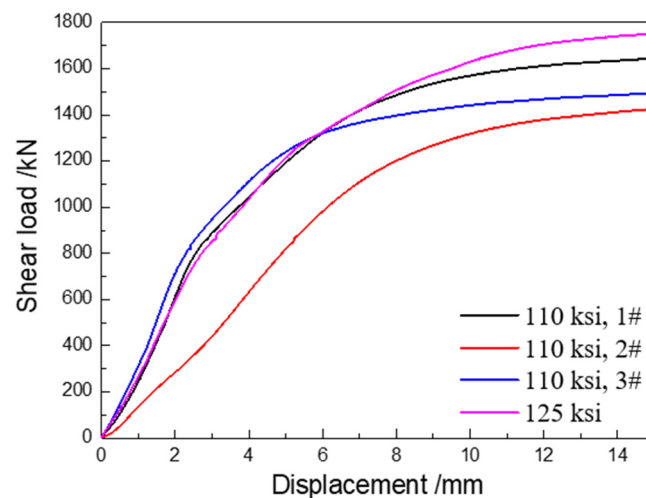


Figure 9. Shear load and displacement curve of cement-sheath casing.

From the above test results, it can be seen that the casing morphology changes under the shear force before and after shear test, and the casing deformation after the shear test is smaller than that of the pure pipe body. The shear load increases with the increase of shear displacement. When the counter-shear is 15 mm, the shear load of 110 ksi cement-sheath casing is 1520 KN and that of 125 ksi casing is 1750 KN. Compared with the pipe shear load, under the action of cement sheath and the same shear displacement, the shear load borne by 110 ksi casing decreases by about 5%, and that of 125 ksi casing decreases by 23%.

4.3. Bearing Characteristics of Pure Casing under Non-Uniform Extrusion Condition

110 ksi ($\phi 139.7 \times 10.54$ mm) and 125 ksi ($\phi 139.7 \times 12.7$ mm) casings are selected for non-uniform external extrusion tests. Two sections of 800 mm-long 110 ksi casing numbered #1 and #2 and one section of 800 mm-long 125 ksi casing are intercepted, and

the “unconventional oil and gas well casing string simulation test system” is used for the non-uniform external extrusion test. The counter extrusion displacement is 20 mm and then the appearance, size and deformation are analyzed. We measure the outer diameter and wall thickness of the casing before the test, and measure the minimum outer diameter of the casing after deformation after the extrusion test. The measurement results are shown in Table 1.

Table 1. Measurement results of casing wall thickness and outer diameter before and after extrusion tests.

Number	Wall Thickness (mm)		Average Value (mm)	Outer Diameter (mm)		Internal Diameter (mm)		Minimum Outer Diameter after Extrusion (mm)	Deformation Value (mm)	Deformation Rate (%)
				Measured	Average	Measured	Average			
110 ksi #1	10.32	10.22	10.23	140.9	140.82	120.44	120.36	109.6	31.22	22.17
	10.1	10.26		140.74		120.28				
110 ksi #2	10.3	10.04	10.25	140.7	140.7	120.20	120.20	109.18	31.52	22.40
	10.26	10.38		140.7		120.20				
125 ksi	13.36	13.22	13.37	140.58	140.51	113.84	113.77	107.96	32.55	23.17
	13.6	13.28		140.44		113.70				

According to the test results, the outer diameters of 110 ksi ($\phi 139.7 \times 10.54$ mm) and 125 ksi ($\phi 139.7 \times 12.7$ mm) casings have become smaller. It is found that the minimum outer diameter of 110 ksi casing is 109.18 mm and the maximum deformation is 22.40%, and those of 125 ksi is 107.96 mm and 23.17%.

The casing shape after the extrusion test is shown in Figure 10, and the relationship between the extrusion load and displacement is shown in Figure 11. It can be seen that the casing morphology changes under external extrusion force. The extrusion load increases with the increase of displacement. When the counter extrusion is 20 mm, the extrusion load of the 110 ksi casing is 1156 KN and that of the 125 ksi casing is 2024 KN.

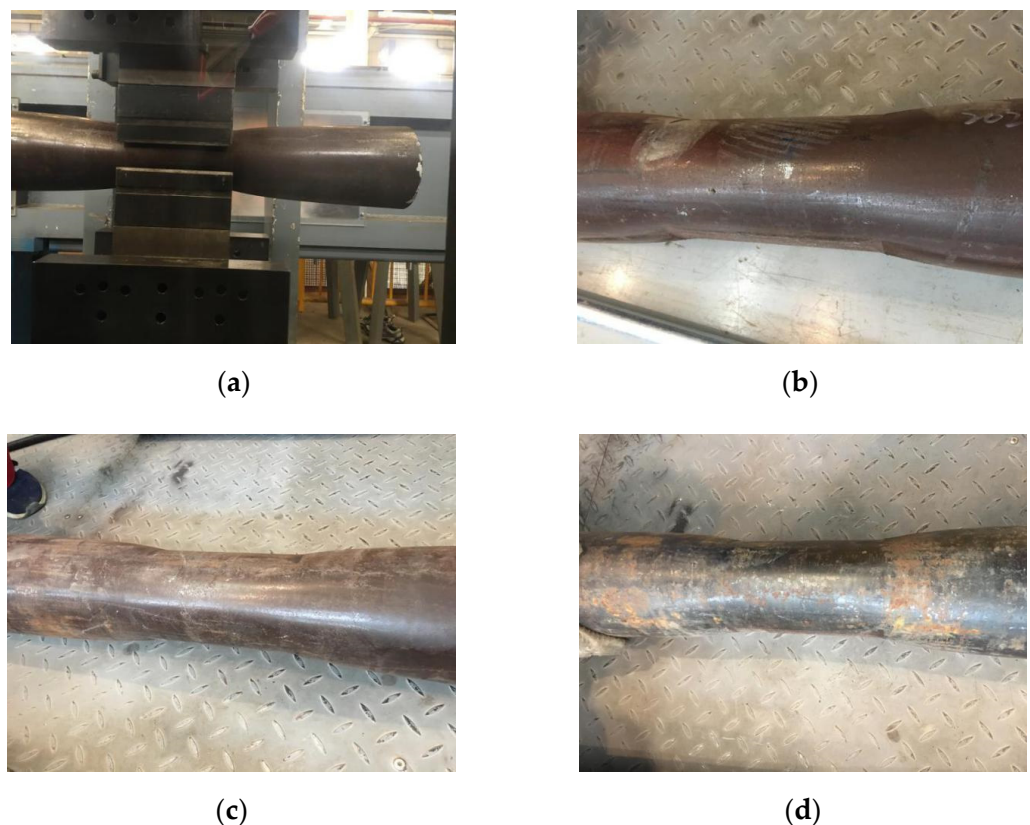


Figure 10. Casing morphology after external extrusion test: (a) extrusion test process; (b) #1 casing appearance after extrusion test; (c) #2 casing appearance; (d) 125 ksi casing appearance.

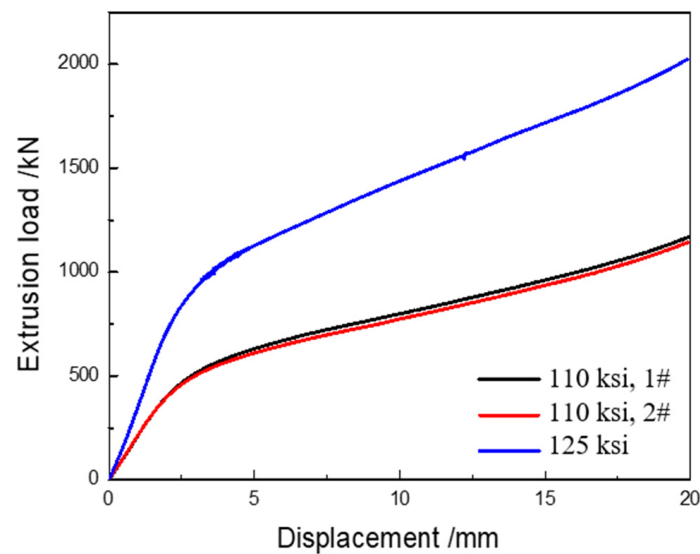


Figure 11. Extrusion load and displacement curve of casing.

4.4. Bearing Characteristics of Cement-Sheath Casing under Non-Uniform Extrusion Condition

After extrusion deformation of 20 mm, the outer diameters of 110 ksi ($\varphi 139.7 \times 10.54$ mm) and 125 ksi ($\varphi 139.7 \times 12.7$ mm) casings become smaller. The minimum outer diameter of 110 ksi casing is 118.6 mm and the maximum deformation is 15.65%, and those of 125 ksi is 124.1 mm and 11.7%. Compared with the pure pipe test, it is found that the deformation value is reduced, indicating that the cement sheath has a certain protective effect on the casing. The finite-element numerical simulation data are studied. Compared with the external extrusion of the pipe, the equivalent stress after adding cement sheath is significantly reduced, and the minimum drift diameter calculated by the same method is 78.21 mm. Compared with 79.28 mm of the pure pipe, the diameter is increased by 1.07 mm, and the deformation of the minimum drift diameter is reduced by 1.35%.

The casing morphology after the extrusion test is shown in Figure 12, and the relationship between the extrusion load and displacement is shown in Figure 13. It can be seen that the cement sheath is damaged, and cracks appear locally under the extrusion force. The extrusion load increases with the increase of displacement. When the counter extrusion is 15 mm, the extrusion load of 110 ksi casing is 3825 KN and that of 125 ksi casing is 4404 KN. Compared with the pure pipe extrusion load, the extrusion load of 110 ksi casing increases by about 230%, and that of 125 ksi casing increases by about 117%.

In conclusion, non-uniform extrusion and shear will cause changes to casing morphology. Under the conditions of extrusion and shear with the same displacement, the diameter deformation of casing protected by cement sheath is smaller, and the minimum drift diameter increase of 125 ksi casing is 1.35% and 1.95%, respectively, indicating that elastic cement sheath has a certain protective effect on casing, but the effect is small. Under the action of a cement sheath, with the same extrusion displacement, the extrusion load of 110 ksi casing increases by about 230%, and that of 125 ksi casing increases by about 117%. At the same shear displacement, the shear load of 110 ksi casing decreases by about 5%, and that of 125 ksi casing decreases by 23%.

Under the condition of 30 mm shear displacement of cement-sheath casing, the inner diameter of 110 ksi casing after deformation is 0.89 mm smaller than that of 125 ksi casing after deformation. Under the conditions of external extrusion load with 40 mm displacement, the inner diameter of 110 ksi casing after deformation is 1.28 mm larger than that of 125 ksi casing after deformation, indicating that the cement sheath has a certain protective effect on the casing.

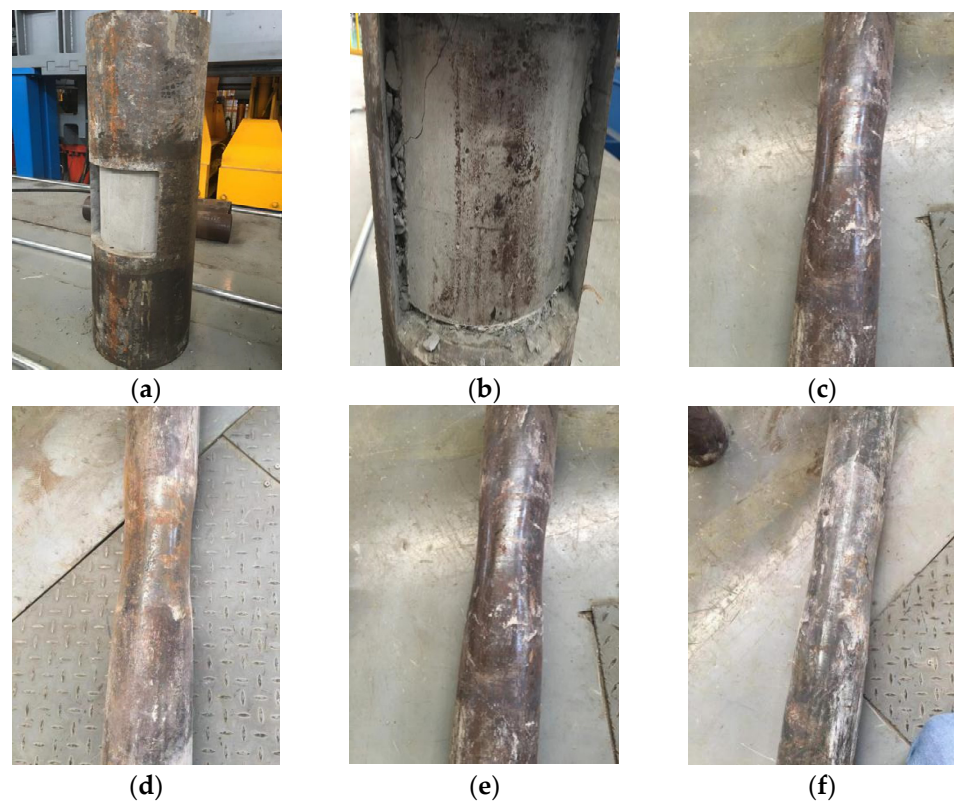


Figure 12. Casing morphology after cement-sheath casing extrusion test: (a) before cement-sheath casing extrusion; (b) after cement-sheath casing extrusion; (c) #1 cement-sheath casing after extrusion; (d) #2 cement-sheath casing; (e) #3 cement-sheath casing; (f) 125 ksi cement-sheath casing.

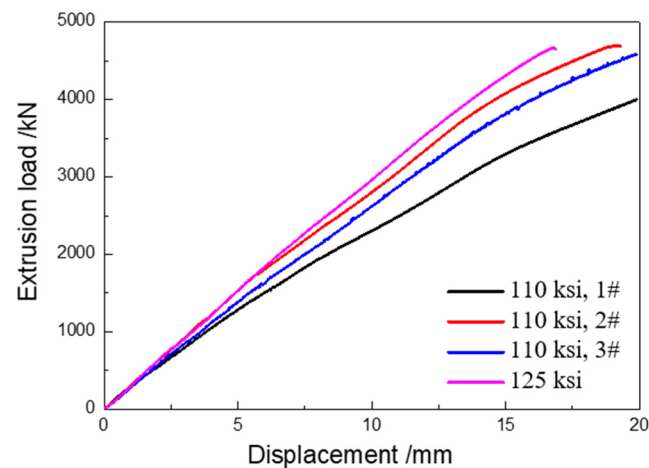


Figure 13. Extrusion load and displacement curve of cement-sheath casing.

4.5. Influence of Thickness and Elastic Modulus of Elastic Cement Slurry

The influence of thickness and elastic modulus of cement slurry on casing deformation is studied. As shown in Figure 14, it is found that with the increase of cement slurry thickness, the deformation of casing gradually decreases. The minimum drift diameter increases, and the absorption of formation slip increases less than 3 mm. When the elastic modulus of cement slurry increases, the deformation of casing gradually increases, the minimum drift diameter decreases, and the formation absorption increases by less than 5 mm. Within the range of the simulation parameters, the deformation of the casing is more sensitive to the elastic modulus than the thickness of the cement slurry, and when the

elastic modulus is less than or equal to 2 GPa, the casing deformation is greatly reduced and the upper end of pipe body is hardly deformed, as described by Yu et al. [18].

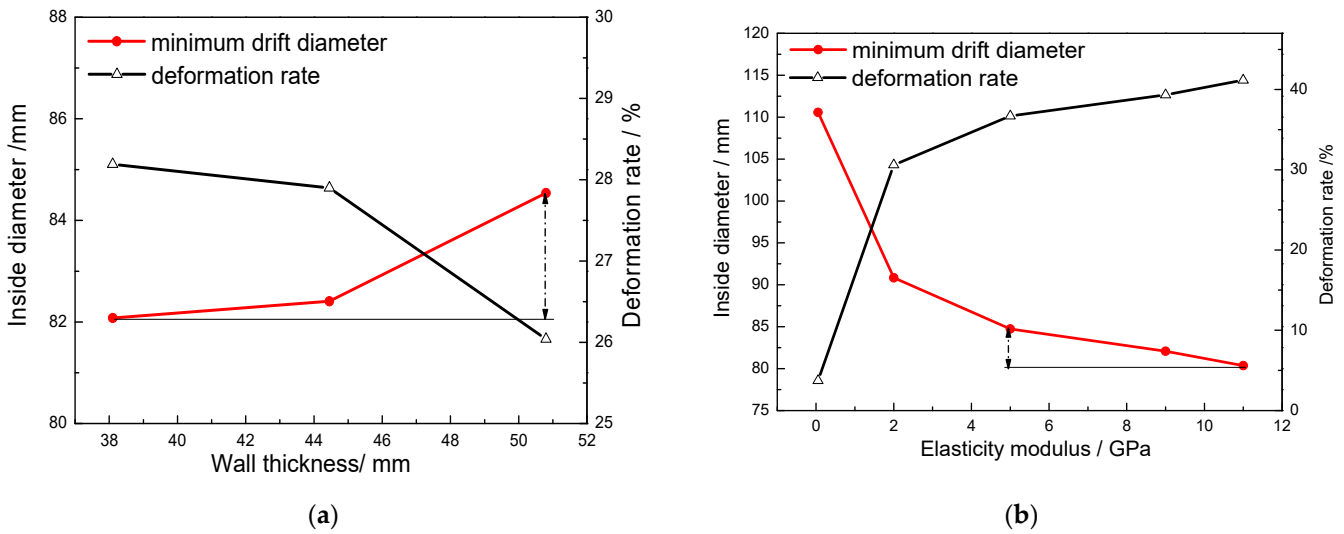


Figure 14. Effect of thickness and elastic modulus of cement slurry on casing inner diameter: (a) wall thickness; (b) elastic modulus.

Due to the complex engineering geological environment, the downhole casing is subjected to various deformation modes such as shear and extrusion under the action of geological strata. Based on the finite-element simulation analysis, the deformation law of cement-sheath casing under the action of shear, single shear and external extrusion is studied, as shown in Figure 15. Under the action of shear, the deformation of cement-sheath casing decreases and the minimum drift diameter increases by 1.45 mm. It shows that the elastic cement sheath has a certain protective effect on the deformation of casing, but a limited ability to absorb deformation.

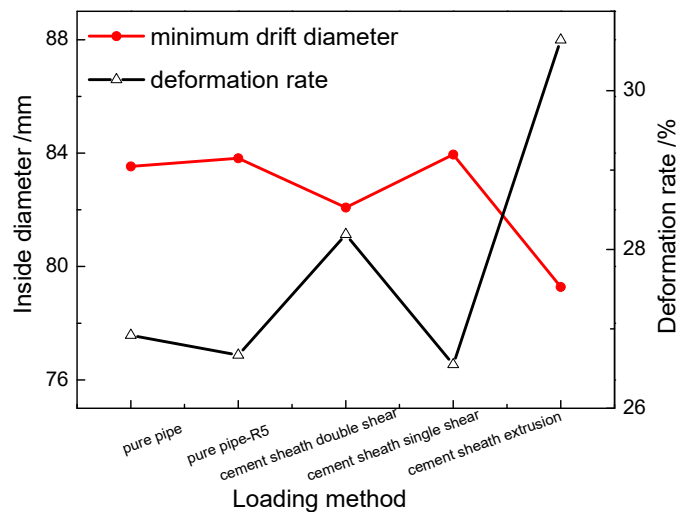


Figure 15. Influence law of different loading methods on casing inner diameter.

Considering the stress concentration at the edges and corners of dies when pure casing is sheared, this paper studies the minimum drift diameter of casing when the die is chamfered (R5), which is reduced by 0.29 mm compared with that without chamfering, indicating that the structure of the die slightly improves the stress uniformity in the cross-section direction of the casing. The upper and lower shear clamps are pressed for 20 mm. Compared with double shear, the deformation in single shear deformation mode is

slightly reduced, and the minimum drift diameter increases by 1.87 mm. Under the action of external extrusion, compared with the shear deformation, the deformation increases significantly under the same counter pressure displacement, and the minimum diameter decreases by 2.8 mm compared with the shear deformation.

5. Non-Uniform Bearing Characteristics of Casing in a Modified Cement Slurry System

Due to the limited deformation absorption capacity of elastic cement slurry, as described by Han et al. [19], a new concept of hollow modification and plasticization of cement sheath is proposed in this paper, which realizes the controllable compression deformation of a high-strength cement sheath, and greatly reduces the casing deformation. A new method of coordinated deformation control of the whole wellbore is established here.

5.1. Simulation Analysis of Crushing Morphology of Modified Cement Slurry

Since the casing deformation mechanism of shale gas horizontal wells is displacement control, and the wellbore system is a closed space, the existing cement slurry system cannot provide space to absorb deformation and the displacement cannot be released. The effect of reducing the elastic cement modulus is not good, and is not easy to realize in engineering. Due to the randomness of the position and size of casing deformation, both the inclined section and horizontal section need prevention and control. Therefore, hollowing of cement sheath can absorb the formation slip based on ensuring the integrity of the wellbore sealing and strength.

Using PFC software, the discrete-element model of modified cement slurry is established, and the crushing forms of cement slurry with formation slip of 5 mm, 10 mm, 15 mm and 20 mm are studied, as shown in Figure 16. The elastic modulus of the modified cement slurry is 2 GPa, the Poisson's ratio is 0.25, and the compressive strength is 18 MPa. When the local layer slides down 5 mm perpendicular to the horizontal casing, all high-strength hollow beads have been deformed to varying degrees, and most of the high-strength hollow beads without elastic–plastic deformation fracture show irregular circular shapes such as ellipses. The broken high-strength hollow beads have lost the original supporting role, making room for stratum slip. When the local layer slides to 10 mm, more high-strength hollow beads are broken and further compacted. When the local layer slides to 15 mm, the high-strength hollow beads at the end are basically broken and compacted. When the local layer slides by 20 mm, the cement sheath doped with high-strength hollow beads is completely compacted.

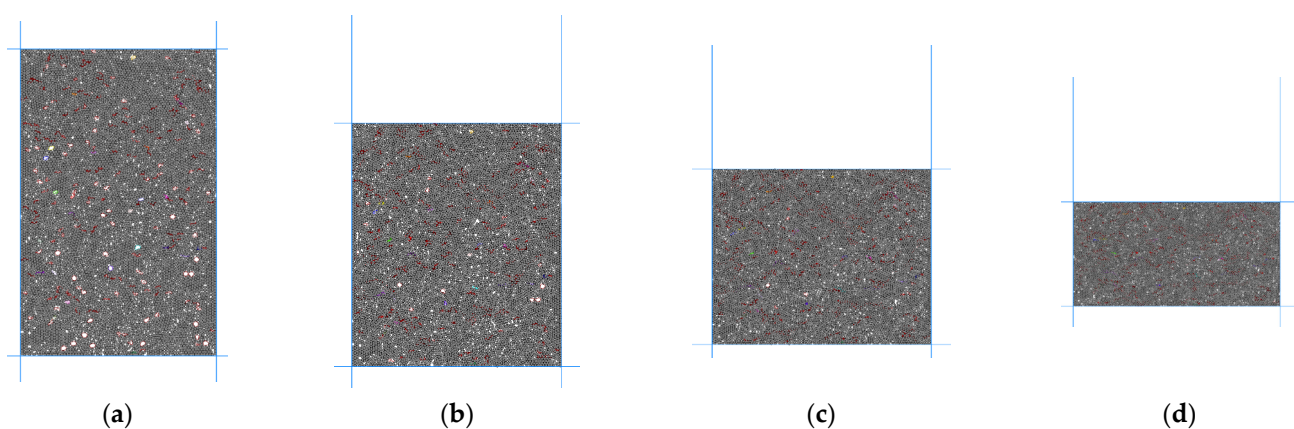


Figure 16. Crushing form of modified cement slurry under different slip amounts: (a) 5 mm; (b) 10 mm; (c) 15 mm; (d) 20 mm.

Figure 17 is the stress curve of a high-strength hollow bead cement sheath doped with different contents transmitting to the casing. The addition of high-strength hollow beads

can reduce the stress transmitted to the casing. When the content of high-strength hollow beads is 0, the stress transmitted to the casing is 98 MPa. When the mixing content is 10%, the maximum stress transmitted to the casing is 66 MPa. When the mixing content is 20% and 30%, the maximum stress transmitted to the casing is 63 MPa and 61 MPa, respectively. With the increase of high-strength hollow bead content, the load on the casing becomes smaller, which can slow down the casing deformation and protect the casing. Furthermore, doping high-strength hollow beads reduces the strength and stiffness of the cement sheath, and the crushing and compaction of high-strength hollow beads frees up the sliding buffer space of the formation.

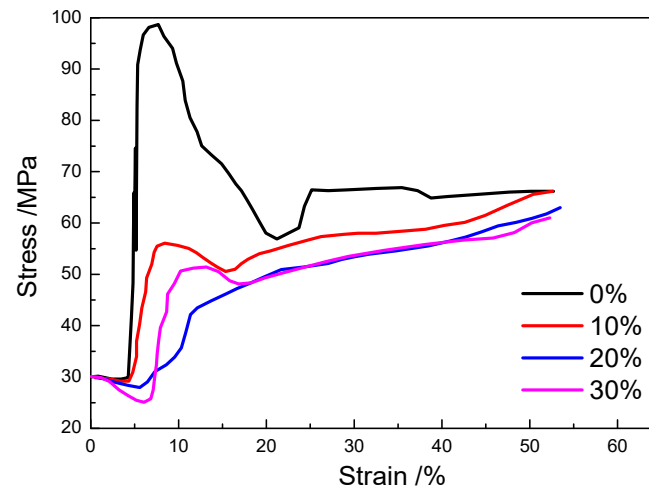


Figure 17. Casing stress transferred by cement sheath added with different high-strength hollow bead proportions.

5.2. Casing Deformation Law with the Modified Cement Slurry

When the formation slides actively, there is cementation between the cement sheath and formation. As the formation has limited slip, the high-strength casing can no longer resist deformation. Using modified cement slurry, the casing deformation can be transferred through the crushing of hollow glass beads. The modified cement sheath wall thickness is set as 38.1 mm. The changes in casing inner diameter under different cementing mud (proportion of high-strength hollow beads) and casing specifications are studied under the condition of 40 mm formation slip. The relationship between formation slip absorption and cement slurry ratio is determined.

Casings of 125 ksi ($\phi 127.0 \times 11.1$ mm, #1~#5) and 125 ksi ($\phi 139.7 \times 12.7$ mm, #6~#10) are selected for non-uniform external extrusion tests. Among them, #1 and #6 are elastic cement slurry, #2 and #7 are cement slurry with 10% high-strength hollow beads, #3, #4, #8, #9 are cement slurry with 20% high-strength hollow beads, and #5 and #10 are cement slurry with 25% high-strength hollow beads. High-strength hollow beads have good compatibility with cement slurry. We analyze the minimum outer diameter and deformation value of the casing after 20 mm extrusion, and results are shown in Figure 18. It can be seen that the deformation value increases with the increase of casing outer diameter and wall thickness. Before the casing plastic deformation, the cement sheath is partially broken and significantly compacted, which can absorb part of the stratum displacement. After the cement sheath is compacted, the casing begins to undergo plastic deformation, and its deformation is significantly lower than that before the cement sheath modification, as shown in Figure 19. The casing deformation can be controlled by adjusting the proportion of cement sheath hollow particles, i.e., the higher the particle content, the smaller the casing deformation. The main reason is that the hollow beads are broken, absorbing part of the loading displacement, reducing the casing deformation and greatly protecting the casing deformation, to realize the active control of the effective drift diameter of casing, and meet the diameter required for engineering fracturing operation.

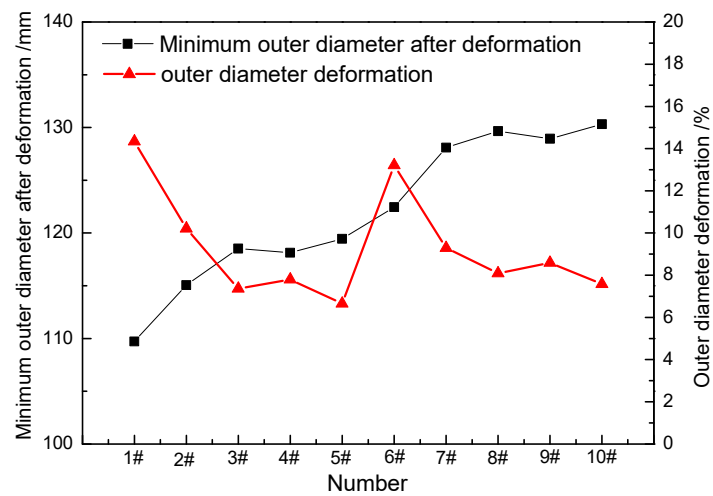


Figure 18. The casing minimum outer diameter and deformation value with modified cement sheath after extrusion.

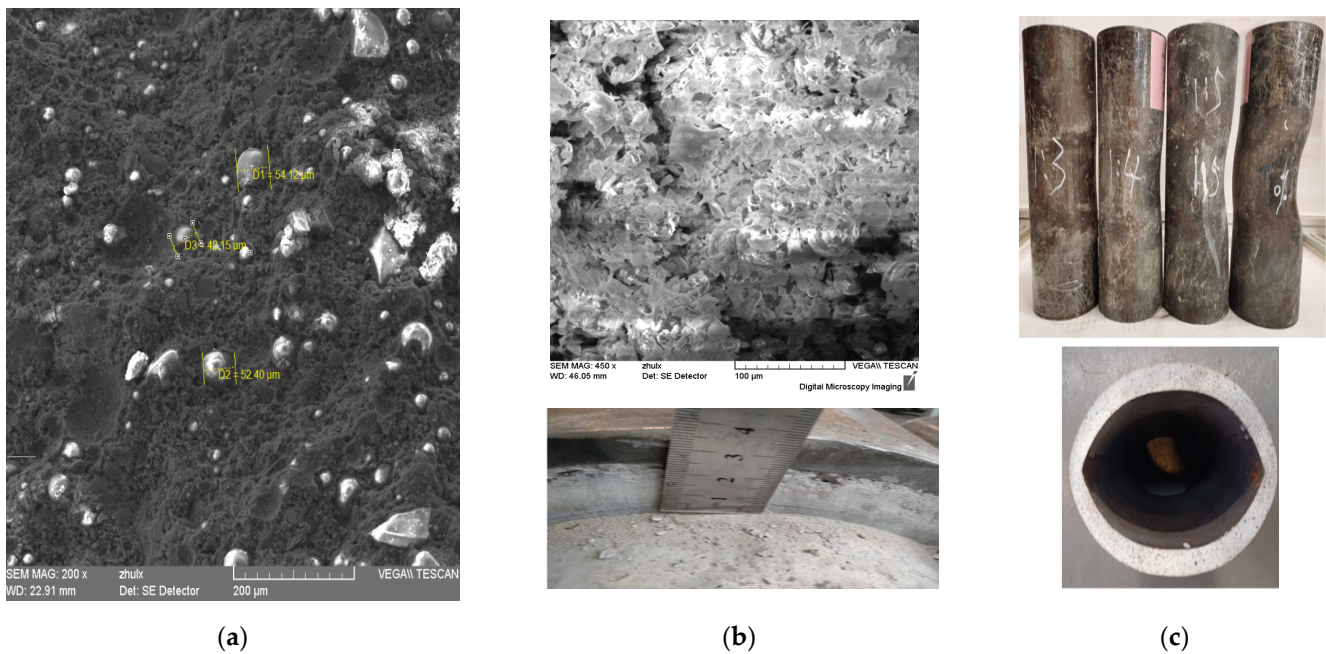


Figure 19. Modification results of cement sheath: (a) morphology of original hollow particles: “D1”, “D2”, “D3” are diameters of three particles; (b) particle crushing morphology; (c) casing deformation relief morphology.

Under shear and extrusion conditions, the casing deformation transfer phenomenon is obvious under the action of modified cement sheath. The relationship between the inner drift diameter of casing and the mass ratio of hollow particles is shown in Figure 20. The local formation slip is 40 mm, for 125 ksi ($\phi 139.7 \times 12.7$ mm) casing, when the mass ratio of hollow particles is 20%. Compared with the elastic cement without addition, the deformation absorbed under shear and extrusion conditions are 17.5 mm and 12.3 mm, respectively, indicating that the modified cement slurry has an obvious effect on absorbing the formation slip, which can realize a large deformation of cement and small deformation of casing. The dotted box is the optimization window through which 99 bridge plugs can pass, which provides guidance for casing transformer control of the cement-sheath casing system. A casing of 125 ksi $\phi 139.7 \times 12.7$ mm and a conventional hollow particle system can absorb less than 27 mm formation slip in total.

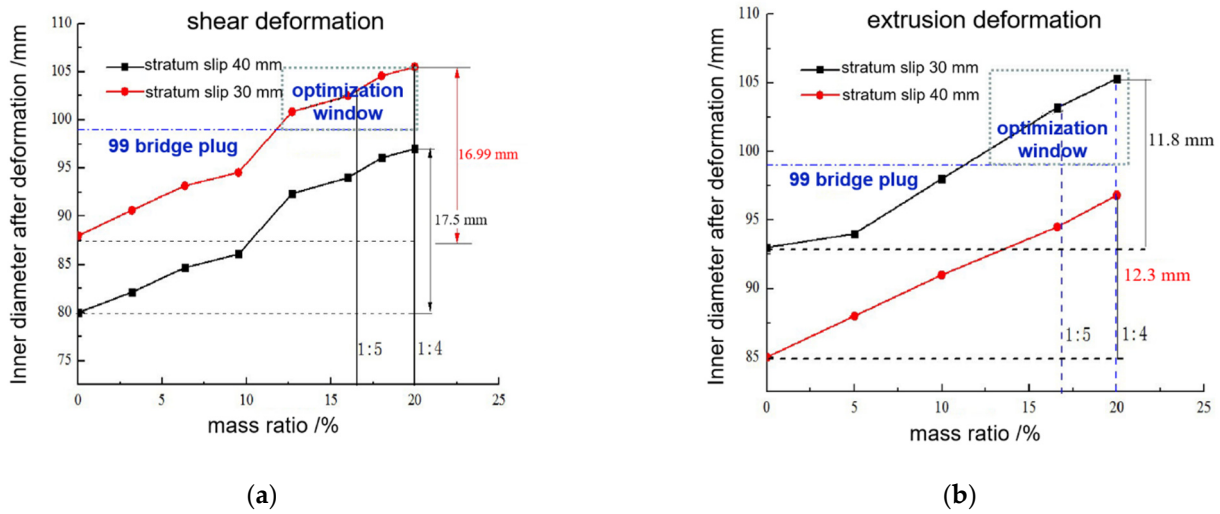


Figure 20. Process optimization window of modified cement sheath: (a) shear deformation; (b) extrusion deformation.

Under the conditions of formation slip, when the ratio of hollow particles and cement slurry is 1:4, the casing deformation transfer phenomenon is obvious. At the initial stage of formation slip (about 10 mm), the force and displacement transmitted to the casing are small, and the casing is not deformed, i.e., the casing inner diameter is not reduced, is considered to be the casing elastic deformation stage, and no obvious plastic deformation occurs. When the formation slip is large, the preventing casing deformation ability of 110 ksi and thick wall casing is weakened, as shown in Figure 21.

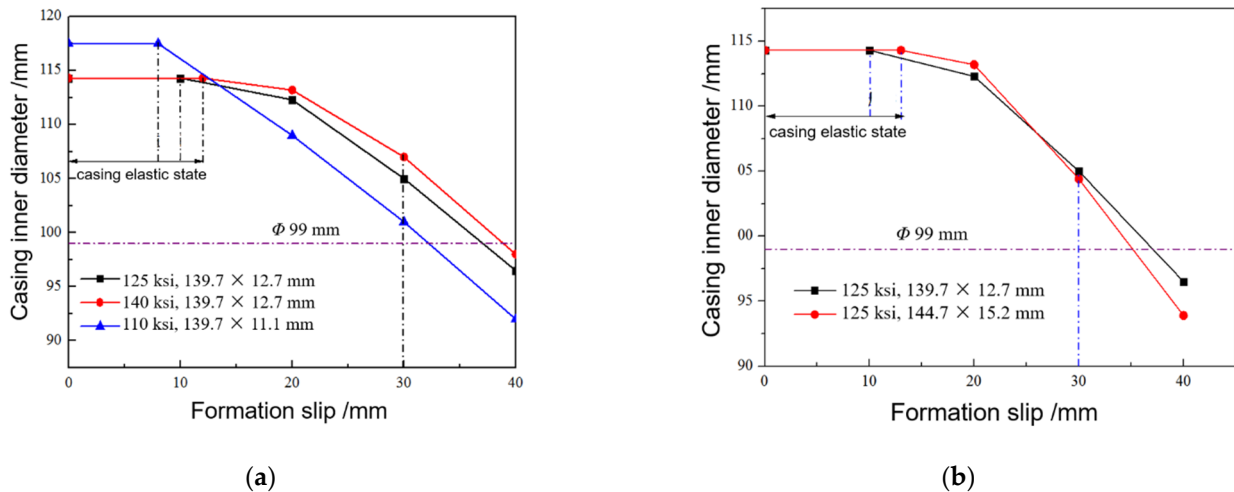


Figure 21. Influence of steel grades and wall thickness on deformation absorption: (a) steel grades; (b) wall thickness.

With the modified cement slurry, good results have been obtained in Weiyuan, Changning, Luzhou and other blocks. At present, there is also a well that is not well cemented, and there is no casing change during fracturing, which also proves that the gap of cement slurry can improve the cementing quality and achieve the purpose of casing change prevention and control.

In future research work, especially for the blocks with serious deformation, further prevention and control measures should be proposed based on the comprehensive consideration of casing running mode, borehole expansion, ductile hollow particles cement slurry and complex fracturing conditions.

6. Conclusions

- (1) The casing deformation mechanism in shale gas wells is formation slip and displacement control, and the slip displacement boundary (<40 mm) under complex fracturing conditions is quantified.
- (2) When the shale reservoir slides, the elastic cement slurry has limited ability to absorb deformation, and the effect of increasing wall thickness and reducing elastic modulus is not obvious. By increasing the wall thickness of the cement sheath (5 1/2" casing), the formation slip absorption increases less than 3 mm. By reducing the elastic modulus of the cement sheath (11→5 GPa), the formation slip absorption increases by less than 5 mm.
- (3) The modified cement slurry provides space for the formation slip absorption, and the effect of casing deformation transfer is obvious. For 125 ksi ϕ 139.7 × 12.7 mm casings, when the formation slip is 40 mm and the mass ratio of hollow particles is 20%, the deformations absorbed under shear and extrusion conditions are 17.5 mm and 12.3 mm, respectively, compared to the elastic cement without addition.

Author Contributions: Writing—Original Draft Preparation, J.C.; Formal Analysis, S.Y.; Funding Acquisition, L.H.; Data Curation, J.W.; Validation, Y.M.; Methodology, C.L. All authors have read and agreed to the published version of the manuscript.

Funding: This research was funded by the supports of Scientific Research and Technology Development of CNPC (2021DJ2705, 2021DJ4403), Study on Key Technologies of Production Increase and Transformation of Gulong Shale Oil (2021ZZ10-04), Innovative Talents Promotion Plan-Young Science and Technology Star Project (2021KJXX-63), Basic Research and Strategic Reserve Technology Research Fund Project of CNPC (2021DQ03 (2022Z-10)).

Institutional Review Board Statement: Not applicable.

Informed Consent Statement: Not applicable.

Data Availability Statement: Not applicable.

Conflicts of Interest: The authors declare no conflict of interest.

References

1. Daneshy, A.A. Impact of off-balance fracturing on borehole stability and casing failure. In Proceedings of the SPE Western Regional Meeting, Irvine, CA, USA, 30 March–1 April 2005; p. 93620-MS.
2. Deenadayalu, C.; Suarez-Rivera, R. The effect of horizontal completions on the breakdown pressures of anisotropic gas shales. *Am. Rock Mech. Assoc.* **2010**, *10*, 27–35.
3. Landry, G.; Welty, R.D.; Thomas, M.; Vaughan, M.L.; Tatum, D. Bridging the gap: An integrated approach to solving sustained casing pressure in the cana woodford shale. In Proceedings of the SPE Well Integrity Symposium, Galveston, TX, USA, 2–3 June 2015; p. 174525.
4. Blake, R. Extending lateral length using casing floatation to reduce field development cost in shale gas plays. In Proceedings of the SPE Annual Technical Conference and Exhibition, Amsterdam, The Netherlands, 27 October 2014.
5. Wang, H.; Liu, H.; Wu, H.A.; Wang, X.X. A 3D numerical model for studying the effect of interface shear failure on hydraulic fracture height containment. *J. Pet. Sci. Eng.* **2015**, *133*, 280–284. [[CrossRef](#)]
6. Hu, C.Y.; Ai, C.; Tao, F.Y.; Wang, F.J.; Yan, M.S. Optimization of well completion method and casing design parameters to delay casing impairment caused by formation slippage. In Proceedings of the SPE/IADC Middle East Drilling Technology Conference and Exhibition, Abu Dhabi, United Arab Emirates, 26–28 January 2016; p. 178144-MS.
7. Casero, A.; Rylance, M. The unconventional unconventional: Tectonically influenced regions, stress states and casing failures. In Proceedings of the SPE Hydraulic Fracturing Technology Conference and Exhibition, The Woodlands, TX, USA, 4–6 February 2020; p. 1997110-MS.
8. Gao, D.L.; Liu, K. Progresses in shale gas well integrity research. *Oil Gas Geol.* **2019**, *40*, 602–615. (In Chinese)
9. Yin, F.; Han, L.H.; Yang, S.Y.; Deng, Y.; He, Y.M.; Wu, X.R. Casing deformation from fracture slip in hydraulic fracturing. *J. Pet. Sci. Eng.* **2018**, *166*, 235–241. [[CrossRef](#)]
10. Yan, W.; Zou, L.Z.; Li, H.; Deng, J.G.; Ge, H.K.; Wang, H.G. Investigation of casing deformation during hydraulic fracturing in high geo-stress shale gas play. *J. Pet. Sci. Eng.* **2017**, *150*, 22–29. [[CrossRef](#)]
11. Liu, K.; Gao, D.; Wang, Y.; Yang, Y. Effect of local loads on shale gas well integrity during hydraulic fracturing process. *J. Nat. Gas Sci. Eng.* **2017**, *37*, 291–302. [[CrossRef](#)]

12. Lian, Z.H.; Yu, H.; Lin, T.J.; Guo, J.H. A study on casing deformation failure during multi-stage hydraulic fracturing for the stimulated reservoir volume of horizontal shale wells. *J. Nat. Gas Sci. Eng.* **2015**, *23*, 538–546. [[CrossRef](#)]
13. Yin, F.; Han, L.H.; Chen, Y.J.; Yang, S.Y.; Shi, B.B. Assessment of Casing Deformation and Optimization of Cement Sheath Performance Under Fracturing Shale Gas Wells. *Pet. Tubul. Goods Instrum.* **2020**, *6*, 41–45. (In Chinese)
14. Bai, L.; Liu, G.; Wang, B.W.; Mei, D. Mechanics-Based Analysis on the 10 3/4" Casing Coupling Section Under Non-Symmetrical Extrusion. In Proceedings of the 29th International Ocean and Polar Engineering Conference 2019, Honolulu, HI, USA, 16–21 June 2019.
15. Li, M.; Liu, J.C.; He, H.Q.; Su, K.H.; Guo, X.L.; Chen, W.Q. Safety and reliability evaluation of casing in ultra-deep well based on uncertainty analysis of extrusion load. *Process Saf. Environ. Prot.* **2021**, *148*, 1146–1163. [[CrossRef](#)]
16. Xu, Z.Y.; Yin, F.; Han, L.H.; Yang, S.Y.; Wu, X.R. Mechanism Study of Casing Deformation in Multistage Hydraulic Fracturing Shale Reservoir. SEG Unconventional Resources Technology Conference 2018, Houston, TX, USA, 23–25 July 2018.
17. Andrade, J.D.; Sangesland, S. Cement Sheath Failure Mechanisms: Numerical Estimates to Design for Long-Term Well Integrity. *J. Pet. Sci. Eng.* **2016**, *147*, 682–698. [[CrossRef](#)]
18. Yu, H.; Lian, Z.; Lin, T. Study on failure mechanism of casing in stimulated reservoir volume fracturing of shale gas. *J. Saf. Sci. Technol.* **2016**, *12*, 37–43.
19. Han, L.H.; Yang, S.Y.; Wei, F.Q.; Ye, X.Q.; Wang, J.J. Casing Deformation Mechanism and Controlling Method for Shale Gas Well Under Complex Fracture Environment. *Pet. Tubul. Goods Instrum.* **2020**, *6*, 16–23. (In Chinese)